Analysis of cloud layer structure in Shouxian, China using RS92 radiosonde aided by 95 GHz cloud radar

Jinqiang Zhang,[1,2] Hongbin Chen,[1] Zhanqing Li,[1,3] Xuehua Fan,[1] Liang Peng,[1,2] Yu Yu,[1] and Maureen Cribb[3]

Received 8 February 2010; revised 28 June 2010; accepted 5 August 2010; published 2 December 2010.

[1] The Atmospheric Radiation Measurement Mobile Facility (AMF) was deployed in Shouxian, Anhui Province, China from 14 May to 28 December 2008. Radiosonde data obtained during the AMF campaign are used to analyze cloud vertical structure over this area by taking advantage of the first direct measurements of cloud vertical layers from the 95 GHz radar. Single-layer, two-layer, and three-layer clouds account for 28.0%, 25.8%, and 13.9% of all cloud configurations, respectively. Low, middle, high and deep convective clouds account for 20.1%, 19.3%, 59.5%, and 1.1% of all clouds observed at the site, respectively. The average cloud base height, cloud top height, and cloud thickness for all clouds are 5912, 7639, and 1727 m, respectively. Maximum cloud top height and cloud thickness occurred at 1330 local standard time (LST) for single-layer clouds and the uppermost layer of multiple layers of cloud. For lower layer clouds in multiple-layer cloud systems, maximum cloud top height and cloud thickness occurred at 1930 LST. Diurnal variations in the thickness of upper level clouds are larger than those of lower level clouds. Multilayer clouds occurred more frequently in the summer. The absolute differences in cloud base heights from radiosonde and micropulse lidar/ceilometer comparisons are less than 500 m for 77.1%/68.4% of the cases analyzed.

Citation: Zhang, J., H. Chen, Z. Li, X. Fan, L. Peng, Y. Yu, and M. Cribb (2010), Analysis of cloud layer structure in Shouxian, China using RS92 radiosonde aided by 95 GHz cloud radar, *J. Geophys. Res.*, *115*, D00K30, doi:10.1029/2010JD014030.

1. Introduction

[2] Cloud vertical structure and the distribution of multi-layer clouds within the atmosphere affects atmospheric dynamics, thermodynamics, and the hydrological cycle, as well as the larger-scale atmospheric circulation through radiative heating/cooling and latent heat release [*Webster and Stephens*, 1984; *Dong et al.*, 2005]. Passive satellite sensors have the advantage of providing global coverage of cloud amounts and top heights, although their retrieval accuracy suffers from various limitations [*Ou et al.*, 1998; *Marchand et al.*, 2001; *Chang and Li*, 2005a, 2005b]. Ground-based active sensors, such as cloud radars, lidars, and ceilometers, can provide cloud measurements with high accuracy and with continuous temporal coverage [*Clothiaux et al.*, 2000; *Dong et al.*, 2000; *Okamoto et al.*, 2008; *Xi et al.*, 2010]. However, these instruments are deployed at few locations around the world. The advent of spaceborne cloud radar and lidar now allows us to see through clouds and to develop cloud vertical structure on a global scale [*Stephens et al.*, 2002; *Mace et al.*, 2009]. Radiosondes can also penetrate cloud layers to provide in situ cloud data. The vertical distributions of temperature, relative humidity (RH) and pressure measured by radiosondes are fundamental to the study of atmospheric thermodynamic and dynamic processes.

[3] Radiosondes of high accuracy and vertical resolution have been widely used to obtain atmospheric parameters. A global network of radiosonde launching stations exists, and data from this network are used as reference for other upper air detection techniques. Methods have been developed to determine the locations of cloud layers and their boundaries from radiosonde measurements [*Arabey*, 1975; *AWS*, 1979; *Dolgin*, 1983]. *Poore et al.* [1995] (hereafter PWR95) used rawinsonde observations to determine the locations of cloud boundaries by testing for dewpoint temperature depressions below some threshold value. *Wang and Rossow* [1995] (hereafter WR95) used radiosonde-measured RH data alone to obtain cloud vertical structure. The radiosonde measures relative humidity with respect to water and temperature at all levels. In WR95, for levels with temperatures lower than 0°C, the RH is computed with respect to ice instead of liquid water. The cloud base and top locations were identified using the following criteria: (1) maximum RH is greater than 87%, (2) minimum RH is greater than 84%, and (3) RH jumps

[1]Key Laboratory of the Middle Atmosphere and Global Environmental Observation, Institute of Atmospheric Physics, Chinese Academy of Sciences, Beijing, China.
[2]Graduate University of the Chinese Academy of Sciences, Beijing, China.
[3]Department of Atmospheric and Oceanic Science and Earth System Science Interdisciplinary Center, University of Maryland, College Park, Maryland, USA.

0148-0227/10/2010JD014030

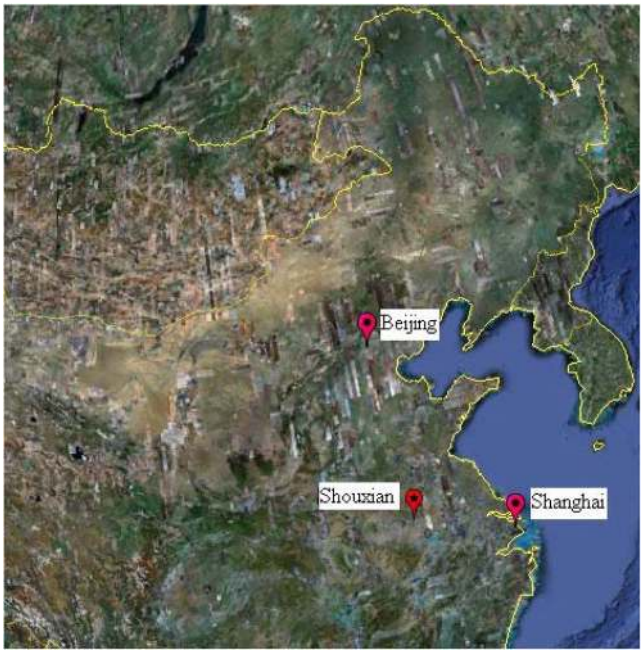

Figure 1. The location of Shouxian.

exceeding 3% are present from the cloud base to the underlying level and from the cloud top to the level above. A limit in the height of the cloud base of the lowest cloud layer was placed and is equal to 500 m. Note that these RH thresholds were modified from 87% to 93% and from 84% to 90% of *Wang et al.*'s [1999] analysis of cloud vertical structure at Porto Santo Island. *Chernykh and Eskridge* [1996] (hereafter CE96) developed a cloud detection method based on the second-order derivatives of temperature and relative humidity with respect to height. The cloud boundaries are defined where at least one of the two second-order derivatives is zero.

[4] *Chernykh et al.* [2000] analyzed the trends in low- and high-cloud boundaries and their errors using radiosonde data obtained from 795 stations around the world. *Minnis et al.* [2005] did a comparison between relative humidity and cloud cover from Vaisala RS80-15LH radiosonde measurements and Rapid Update Cycle (RUC) data taken over Atmospheric Radiation Measurement's (ARM) Southern Great Plains (SGP) Central Facility (SCF). They found that both types of data could be used to estimate the occurrence of clouds, although radiosonde data appear to be more reliable than RUC data. *Naud et al.* [2003] used lidar and ceilometer data collected at the SCF from November 1996 to October 2000 to assess the retrievals of WR95 and CE96. The agreement between cloud radar and radiosonde-derived cloud boundaries was better for cloud base heights than for cloud top heights. Overall, WR95 tended to misclassify moist cloudless atmospheric layers as clouds, and both radiosonde techniques reported higher cloud tops than those from cloud radar. By using radiosonde data, *Wang et al.* [2000] provided a global picture of cloud vertical structure and found that the average values for cloud base height, cloud top height, and cloud layer thickness were 2.4 km above mean sea level (MSL), 4.0 km MSL, and 1.6 km, respectively. *Wang and Rossow* [1995] analyzed radiosonde data at 30 marine sites and reported that, under cloudy conditions, multilayered clouds occur most frequently (56%) and are predominately two layered. However, few works have been published concerning cloud structure in China based on radiosonde data. Work that has been done on the subject involved analyses of a limited number of cases, and the quality of the results was not examined through comparisons with observations from other instruments. The mean vertical resolution of radiosonde data has changed over the years. Before 1970, the vertical resolution was 50 hPa, and from 1970 to 1980, the vertical resolution was improved to 30 hPa. The method developed by WR95 used radiosonde data with low vertical resolution. The Vaisala RS92 radiosonde measures data every 2 s with an average ascent rate of about 5 m/s, resulting in a much higher vertical resolution (10 m: 5 m/s × 2 s).

[5] Until the deployment of the Atmospheric Radiation Measurement Mobile Facility (AMF) in China (referred to as AMF-China hereafter) 2 years ago, no high-resolution radiosonde data or cloud radar measurements existed to study cloud structure in China. This study presents the first attempt at examining cloud vertical structure in China.

[6] Section 2 describes the data and the method employed in this study. The characteristics of cloud vertical structure are discussed in section 3. The diurnal variation and seasonal (summer-autumn) differences are also analyzed. Cloud structure obtained from radiosonde data are compared to those detected by the W band ARM cloud radar (WACR), the micropulse lidar (MPL), and the Vaisala ceilometer, and results are presented in section 4. Main conclusions are summarized in section 5.

2. Data and Analysis Method

2.1. Data Description

[7] Sponsored by the DOE's ARM program, the AMF was deployed in Shouxian, Anhui Province (32.56°N, 116.78°E, 21 m above sea level) from 14 May to 28 December 2008, in cooperation with the Institute of Atmospheric Physics of the Chinese Academy of Sciences, the Meteorological Observation Center, and the Anhui Meteorological Bureau, China Meteorological Administration. Shouxian, as shown in Figure 1, is located approximately 500 km west of Shanghai, in the Jiang-Huan prairie region between the Huai and Yanzi rivers. The site is located at the edge of a rural town with a population of ~50,000 and is largely surrounded by farmland. Its weather is influenced by the East Asian monsoon system. The mobile facility was developed in 2005 to supplement fixed site operations at the SGP, tropical Western Pacific (TWP), and North Slope of Alaska (NSA) regions and can be deployed anywhere in the world on a 6 month to 1 year basis.

[8] During the entire study period, Vaisala RS92 radiosondes were launched 4 times a day (0530, 1130, 1730, and 2330 UTC) without any major interruption. Eight-hundred forty-two launches were made in total, of which 96.6% and 73% reached altitudes greater than 10 and 20 km, respectively. The Vaisala RS92 radiosonde, which has a high interference-resistant ability, accuracy, and temporal resolution (2 s), collected profiles of temperature, RH, pressure, wind speed, and direction.

[9] The W Band Atmospheric Radiation Measurement (ARM) Program Cloud Radar (WACR) is a zenith-pointing Doppler radar that probes the extent and composition of

clouds at 95 GHz with a minimum range resolution of 45 m. WACR can detect cloud boundaries up to 15 km.

[10] The micropulse lidar (MPL) is a ground-based lidar system of one channel at 532 nm that records backscatter signals up to 20+ km, with a 30 m resolution. From the relative backscattering signal, it is possible to determine cloud boundaries for thin clouds and cloud base for all clouds, as well as aerosol extinction and backscatter coefficients up to 18 km every 3 or 4 s with a precision of ±15 m.

[11] The Vaisala ceilometer (VCEIL) is a low-energy lidar at a wavelength of 905 nm designed chiefly for detecting cloud base heights with some potential for probing aerosols as well. The product used here are quality-controlled cloud base with a vertical resolution of 15 m and a temporal resolution of 15 s. Five detection flags are included: no significant backscatter (0), one cloud base detected (1), two cloud bases detected (2), three cloud bases detected (3), full obscuration determined but no cloud base detected (4), and some obscuration detected but determined to be transparent (5).

[12] Both MPL and VCEIL cannot penetrate thick low-level clouds to detect any other more layers of clouds aloft. However, they are excellent for detecting all clouds that are visible from the ground within their observation ranges [*Clothiaux et al.*, 2000]. The greatest strength of the WACR is its ability to penetrate clouds and reveal multiple-layer clouds but may miss some thin clouds composed of small hydrometeors. Yet the detection of cloud base heights from radar is often affected by the presence of large precipitation particles, as well as insects and bits of vegetation. They are commonly suspended in the atmospheric boundary layer, which may be mistakenly regarded as stratus clouds.

2.2. Analysis Method

[13] The methods presented in WR95 determine cloud locations from relative humidity profiles and use the same minimum and maximum RH thresholds of 84% and 87%, respectively, for all altitudes. These relative humidity profiles are sampled at least every 200 m. For levels with temperatures lower than 0°C, the RH is computed with respect to ice instead of liquid water. The RH profile is examined from the surface upward to find cloud layers in five steps: (1) the base of the lowest moist layer is determined as the level that satisfies the two conditions: (a) minimum RH at least 84% and (b) RH increases at least 3% from the adjacent lower level; (2) RH is at least 84% above the base of the moist layer; (3) the top of the moist layer is identified when RH decreases by more than 3% and is lower than 84%; (4) the moist layer is classified as a cloud layer if the maximum RH within this layer is more than 87%; and (5) minimum cloud height is set to 500 m above ground level (AGL). Five hundred meters is chosen as the lowest possible cloud base height, because according to statistics compiled by ground observers, low clouds have a mean base height of 512 ± 148 m. For "single-level" clouds having the same level identified as top and base, cloud layer top is assigned as half the distance to the next level above and the base is at half the distance to the next level below.

[14] The method used in WR95 was modified for use in the analysis of cloud vertical structure over the Shouxian region. Without knowledge of the transforming formula in WR95, in our analysis, the RH is computed with respect to ice instead of liquid water for levels with temperatures lower than 0°C following the relation proposed by *Alduchov and Eskridge* [1996]. The condition that RH jumps over 3% at the cloud base and top in WR95 can be easily satisfied, because the method developed in WR95 was based on radiosonde data with low vertical resolution. As *Wang* [1997] stated, minor variations in cloud base-top and cloud base heights occur when the RH jumps changed from 3% to 0% or from 3% to 6%. The method used in RS92 employed radiosonde data with much higher vertical resolution (2 s). The average radiosonde ascent is about 5 m/s. With this vertical resolution, the distance from the level below to cloud base and from cloud top to the level above is about 10 m (5 m/s × 2 s). The RH 3% jump threshold at cloud base and top is difficult to meet within such a short distance, so this test is discarded. The limitation on minimum cloud thickness for low and middle/high clouds was more than 30.5 and 61.0 m in PWR95, respectively, but there was no limitation on cloud thickness in WR95. To reduce the possibility of misclassifying thin clear moist layers as clouds, the minimum thickness limitations described in PWR95 are kept. For the reason of high vertical resolution data from RS92, the single-level, defined as in WR95 analysis, is about 10 m in thickness. Thus, in our analysis, the single-level cloud layers are excluded by the minimum thickness limitations mentioned above. For a field of scattered cumulus clouds, RH may be lower when a radiosonde passes through a cloud gap. So it is possible to misclassify a cloud layer consisting of scattered clouds as multilayer clouds using the minimum RH thresholds (hereafter min-RH) and maximum RH thresholds (hereafter max-RH). To reduce this possibility, if the distance between two contiguous layers is less than 300 m or the minimum RH within this distance (hereafter inter-RH) is slightly less than min-RH, the two layers are considered as one-layer cloud.

[15] Setting the lowest cloud base at 500 m AGL, as in WR95, may not be applicable for data from Shouxian, because this value was based on observations from another location. A more suitable value was found using ceilometer data collected at Shouxian. Because of its high resolution, ceilometer data are generally used to retrieve base heights of low-altitude clouds. The highest frequency is at about 280 m for cloud bases lower than 500 m from ceilometer data at Shouxian. However, the lowest cloud base height from the MPL preliminary cloud base product is about 450 m. Given the higher vertical resolution of ceilometer data, the lowest cloud base height is set at 280 m. Shouxian is located in southern China, which is humid during the rainy warm season. Moist layers near the surface are associated with fog, drizzle, or rain. Given the difficulty in discriminating these hydrometeors from sounding data, they are discarded in our statistics. To remove these near-surface moist layers with no clouds, moist layers with bases lower than 120 m and thicknesses less than 400 m are excluded.

[16] The WR95 method is able to detect virtually all low clouds, but with a large commission error of about 10%. Five percent of the time, the method classified some cloud-free moist layers as clouds and missed high and thin clouds [*Wang*, 1997]. In order to overcome the problem of false detection near the surface, *Wang et al.*'s [1999] method increased the RH thresholds at the bottom and top of a potential cloud layer from 84% to 90% and from 87% to 93%, respectively. *Naud et al.* [2003] speculated that better cloud

Table 1. Summary of Height-Resolving RH Thresholds

Altitude Range	Height-Resolving RH Thresholds		
	min-RH	max-RH	inter-RH
0–2 km	92%–90%	95%–93%	84%–82%
2–6 km	90%–88%	93%–90%	80%–78%
6–12 km	88%–75%	90%–80%	78%–70%
>12 km	75%	80%	70%

boundaries might result from the WR95 study if the RH thresholds were larger at low altitudes and smaller at high altitudes. *Slingo* [1980] defined different thresholds for low-, mid-, and high-level clouds for a numerical model cloud parameterization. Analyzing ceilometer and radiosonde RH data for broken clouds at the ARM SGP site, *Han and Ellingson* [2000] found that the RH threshold decreases at cloud base as the altitude of the cloud increases at least up to heights of 2.5 km. *Chernykh* [1999] confirmed that this holds for all cloud layers. It is thus necessary to take into account the altitude dependence of RH at cloud bases in order to determine cloud boundaries more accurately. To this end, the min-RH, max-RH, and inter-RH are set to decrease linearly with height, and their values are shown in Table 1.

[17] The modified cloud detection algorithm is thus summarized as follows using the height-resolving threshold of max-RH, min-RH, and inter-RH values specified in Table 1. Before applying any test, RH is first transformed with respect to ice instead of liquid water for all levels with temperatures below 0°C, which is then examined to identify cloud layers in eight steps: (1) the base of the lowest moist layer is determined as the level when RH exceeds the min-RH corresponding to this level; (2) above the base of the moist layer, contiguous levels with RH over the corresponding min-RH are treated as the same layer; (3) the top of the moist layer is identified when RH decreases to that below the corresponding min-RH or RH is over the corresponding min-RH but the top of the profile is reached; (4) moist layers with bases lower than 120 m and thicknesses less than 400 m are discarded; (5) the moist layer is classified as a cloud layer if the maximum RH within this layer is greater than the corresponding max-RH at the base of this moist layer; (6) the base of cloud layers is set to 280 m AGL, and cloud layers are discarded if their tops are lower than 280 m; (7) two contiguous layers are considered as a one-layer cloud if the distance between these two layers is less than 300 m or the minimum RH within this distance is more than the maximum inter-RH value within this distance; and (8) clouds are discarded if their thicknesses are less than 30.5 m for low clouds and 61 m for middle/high clouds.

[18] A summary of the tests used in WR95 and in this study is given in Table 2.

3. Analysis of Cloud Layers Determined From Radiosonde Profiles

3.1. Vertical Distribution of Cloud Layers

[19] The modified method was applied to data from radiosonde launches, which had a maximum detection altitude of over 10 km. A total of 1363 cloud layers were identified in Shouxian during the AMF deployment. The average RH gradients at the cloud base and top are 1.4% and −3.1% per 10 m, respectively. The frequency distribution of maximum observation altitudes is shown in Figure 2a, and the numbers of occurrence for single-layer and multilayer clouds are shown in Figure 2b. Cloud-free cases and one to three cloud layers account for 21.5%, 28.0%, 25.8%, and 13.9% of all cases, respectively. The rest (about 11%) are cases where there are more than three cloud layers.

[20] Clouds are classified into four groups: (1) low clouds with bases lower than 2 km and thicknesses less than 6 km; (2) middle clouds with bases ranging from 2 to 5 km; (3) high clouds with bases greater than 5 km [*Lazarus et al.*, 2000]; and (4) vertically developed clouds (hereafter called deep convective clouds) with bases less than 2 km and thicknesses greater than 6 km. These four types of clouds account for 20.1%, 19.3%, 59.5%, and 1.1% of all cloudy cases, respectively. High clouds occurred most frequently.

[21] The mean vertical locations and cloud thicknesses for the four types of clouds are shown in Figure 3. Except for the deep convective clouds, the middle clouds are thickest (~2200 m), and the thicknesses of low and high clouds are similar.

[22] The average cloud base height, cloud top height, and cloud thickness for one to three cloud layers are shown in Figure 4. Note that single-layer clouds are generally located at altitudes that fall somewhere between the altitudes of the two- and three-layer cloud configurations. Single-layer clouds are thicker than the cloud layers forming multilayer clouds with a mean difference of −867 m, and upper layer clouds are thicker than lower layer clouds in multiple-layer cloud configurations. This may be due to interactions between the different layers of cloud. This feature might also be associated with the strong reduction in longwave radiative (LW) cooling at the top of the lower layer of cloud in the presence of upper layers of cloud [*Wang et al.*, 1999; *Chen and Cotton*, 1987].

[23] Cloud layers with thicknesses less than 2 km occurred most frequently for all clouds. For single-layer clouds and the upper layer of two-layer clouds, the majority of cloud bases range from 5 to 9 km, respectively. The majority of cloud top heights for single-layer clouds and the upper layer of two-layer clouds range from 7 to 12 km. In the two-layer cloud configuration, the thickness of the upper level cloud layer is larger than that of the lower level cloud. The thicknesses of upper level clouds are about the same as those of single-layer clouds. In the three-layer cloud configuration, the base and

Table 2. Summary of the Cloud Determination Method Presented in WR95 and the Modified Method Used in This Study

Judgments Methods	WR95	Modified Method
Height resolution of radiosonde data	Low	High
Max-RH, Min-RH	The same at all altitudes	As a function of altitude
RH jump at cloud base/top	3%	–
Judgment of two contiguous layers	–	Judged by the distance or inter-RH
Lowest cloud base	500 m	280 m
Thickness for low/(middle and high) clouds	–	30.5/61 m
Single layers	Kept	Discarded

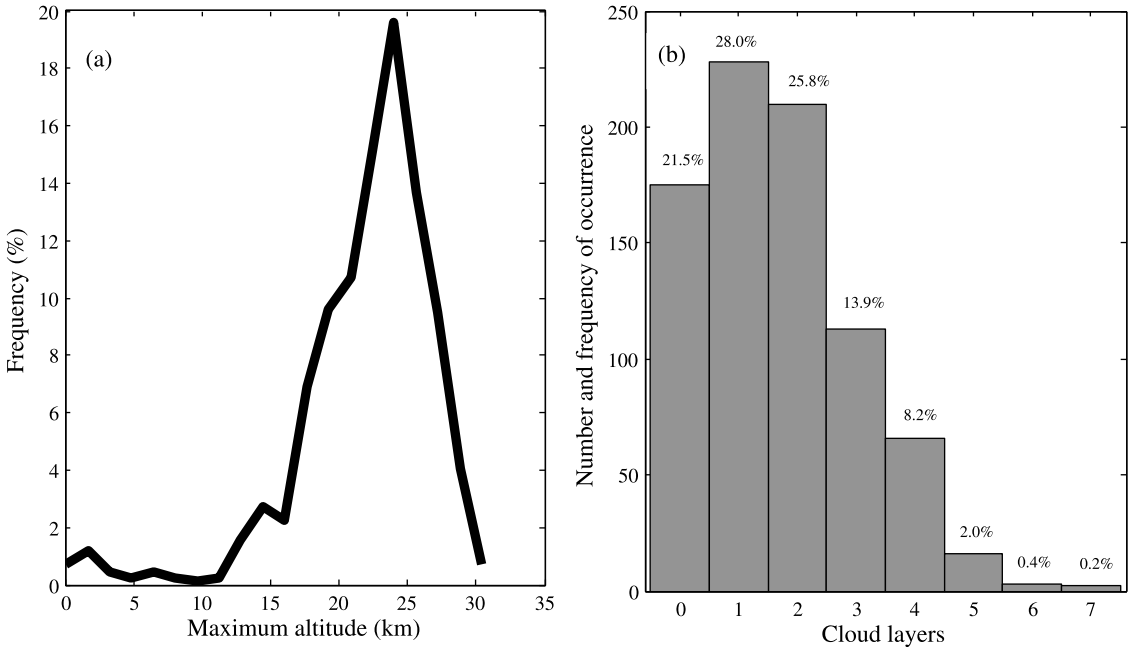

Figure 2. (a) Frequency distribution of maximum altitudes attained by radiosondes after launch. (b) Frequency of occurrence and percentage of different cloud layers.

top heights of the lowest layer of cloud are similar to those of the lowest layer of cloud in a two-layer cloud configuration.

3.2. Diurnal Variations of Cloud Layers

[24] Much research has focused on the diurnal variation of cloud layers [*Wang et al.*, 1999; *Minnis and Harrison*, 1984; *Blaskovic et al.*, 1991; *Dong et al.*, 2006]. Along the same vein, the diurnal variation of cloud layers at the AMF-China is also studied and is based on measurements from four radiosonde launches per day. The average diurnal variations for one-layer clouds, two-layer clouds, and three-layer clouds are shown in Figures 5a–5c, respectively.

[25] The most notable variations for single-layer clouds and the uppermost layer of multiple layers of cloud occur between 1330 local standard time (LST) and 1930 LST, with cloud tops and thicknesses reaching a maximum at 1930 LST. The lower layers of cloud in multiple-layer cloud configurations show the greatest variations between 730 LST and 1330 LST, with cloud tops and thicknesses reaching a maximum at 1330 LST. The thickness variations are larger in

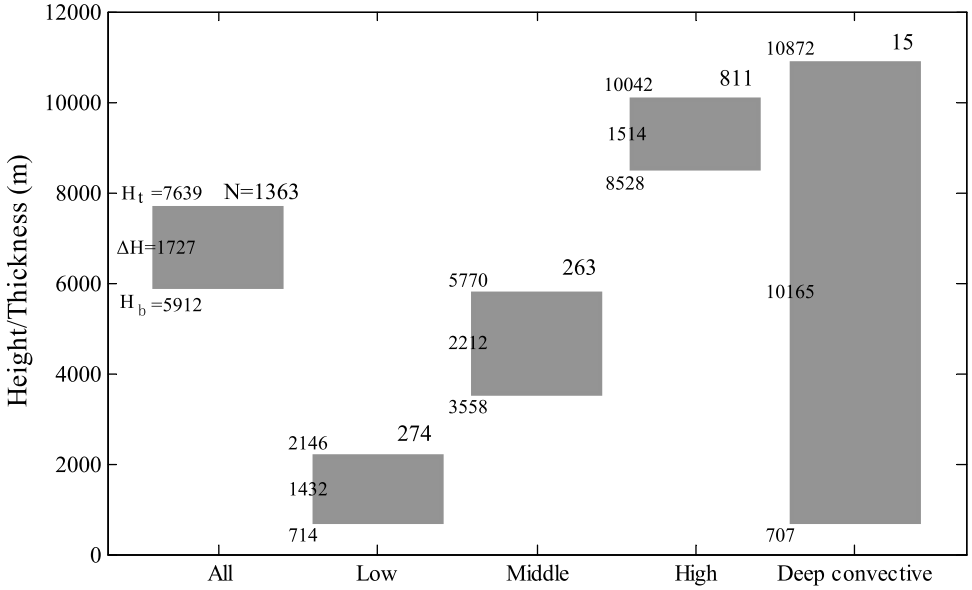

Figure 3. Mean locations and thicknesses of all cloud layers, low cloud layers, middle cloud layers, high cloud layers, and deep convective clouds. H_b, H_t, ΔH (units in m), and N are the mean cloud base height, mean cloud top height, mean thickness, and number of each type of cloud, respectively.

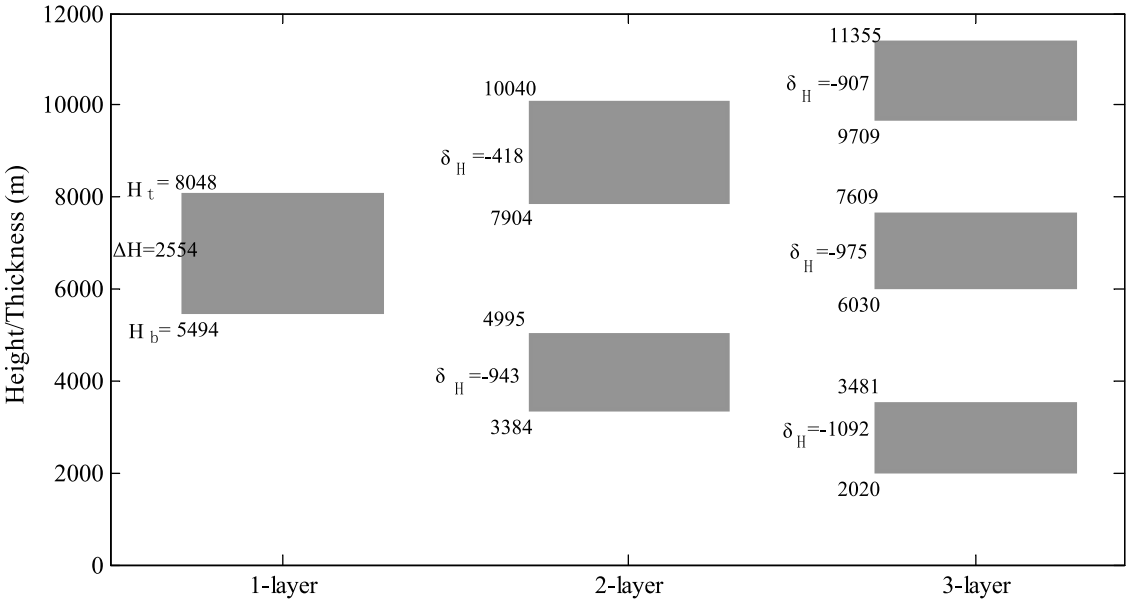

Figure 4. Mean locations of one-, two- and three-layer clouds. H_b and H_t are the mean cloud base height and cloud top height for each cloud type, respectively. ΔH is the mean thickness of one-layer clouds; δ_H is the difference in thickness between each layer of cloud in a multilayer cloud configuration and one-layer clouds. Units are in meters.

the uppermost layers of cloud than in the lower layers of cloud when multiple layers of cloud are present. The following hypothesis is put forward here in an attempt to explain the observed phenomenon from the perspective of radiative energy exchanges that affect the thermodynamic state of cloud layers. While realizing that dynamics play an important role in cloud development, we believe that for long-term mean results presented here, radiative effects are more dominant. From the viewpoint of thermodynamics, cloud maintenance and development is also modulated by adiabatic processes, namely solar heating and longwave (LW) radiative cooling. The important role of radiative effects in the evolution of various clouds was investigated by *Guan et al.* [1997]. Near noontime (~1330 LST), solar heating is so strong that

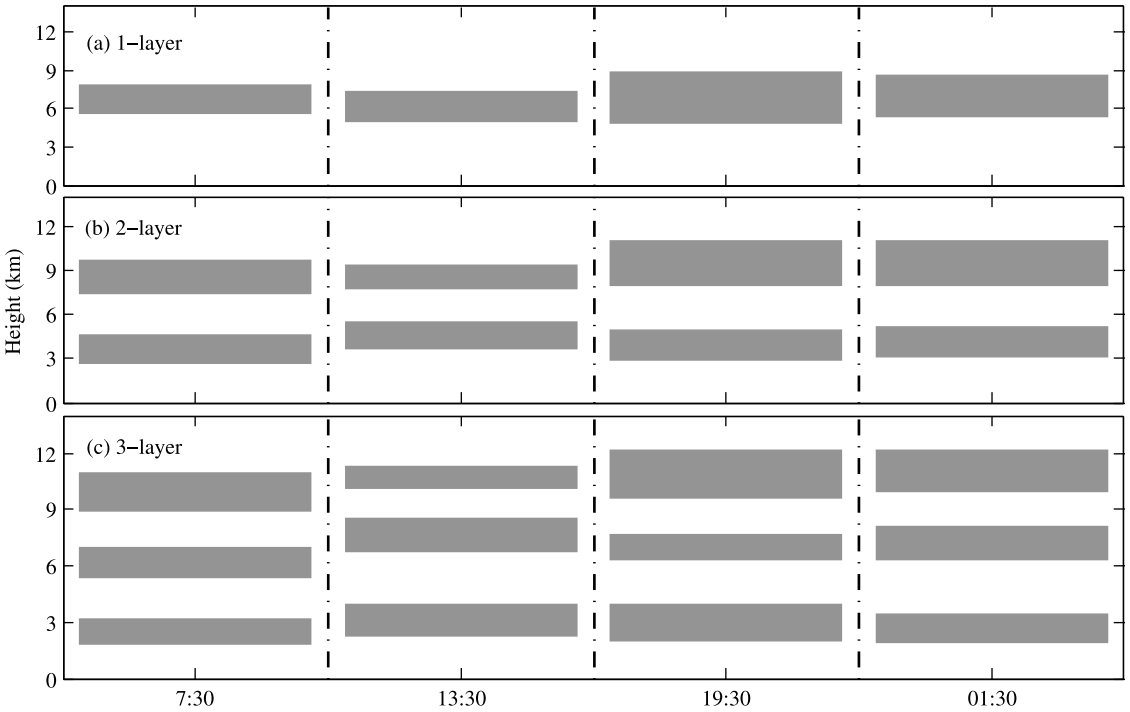

Figure 5. Diurnal variations of one-, two-, and three-layer clouds.

Table 3. Cloud Layer Frequency in Summer and Autumn

Season	Number of Radiosonde Launches	Total Number of Cloud Layers Detected	Number of One-Layer Clouds	Number of Two-Layer Clouds	Number of Three-Layer Clouds
Summer	369	741	79	105	61
Autumn	369	485	115	80	40
Summer-Autumn[a]	0	256	−36	25	21

[a]Summer-autumn is the difference between summer and autumn observations.

(1) evaporation of cloud drops may occur and (2) atmospheric stability may increase thus suppressing cloud development. These damping effects were also demonstrated by *Rogers and Koracin* [1992]. So near noontime, the vertical development of single-layer clouds and the vertical development of the uppermost layer of multiple layers of cloud are suppressed due to solar heating. However, for lower layers of cloud in a multiple-layer cloud configuration, solar heating is greatly reduced because of the absorption and scattering processes of the upper layers of cloud. The ground surface is warmer than any cloud layer so through the exchange of LW radiation, the cloud base gains more energy. This facilitates cloud development and leads to a maximum in cloud altitude and thickness at 1330 LST. As the Sun sets, LW radiative cooling starts to dominate over shortwave (SW) radiative warming. Cloud top temperatures begin to lower, which increases atmospheric instability and fuels the development of single-layer clouds and the uppermost layer of cloud in multiple-layer cloud configurations. At sunset, solar heating diminishes and LW cooling strengthens, which may explain why there is a peak at 1930 LST in the location of the cloud top of single-layer clouds and the uppermost layer of multiple layers of cloud. The resulting stability dampens the development of lower layers of cloud between 1330 LST and 1930 LST. For multilayer clouds, the magnitude of LW energy exchange between the layers is much smaller than between clouds and the surface, which may explain why low-level cloud top heights decrease with increasing number of cloud layers, as shown in Figure 5. The exchange of LW radiation between a cloud base and a lower level cloud or the surface also helps explain why there is no peak in cloud top height at night. Continual cooling of cloud tops due to LW emission would increase atmospheric instability during the nighttime. This effect is weakened by the decreasing gain of LW energy at the cloud base due to the cooling of the surface or the cloud top of the lower clouds. Modeling studies may confirm this hypothesis.

3.3. Comparison of Cloud Layers Occurring in Summer and Autumn

[26] In order to analyze cloud variations in different seasons, cloud layer configurations in summer and autumn are compared. Summer observations are defined as observations made during the months of June, July, and August and autumnal observations are defined as observations made during the months of September, October, November, and the first half of December. An instrument breakdown occurred during the middle of September so observations made in December are included in order to cover the same amount of time as summer observations. The average, maximum, and minimum temperatures in November are 11.7°C, 25.8°C, and −3.5°C, respectively, and for the first half of December, they are 7.6°C, 22.7°C, and −5.2°C, respectively. Given the small change in temperature during these two periods, it is reasonable to substitute missing observations in September with those from the first half of December. Cloud layer frequencies during the two seasons are given in Table 3.

[27] There are a greater number of cloud layers present during the summer than during the fall, suggesting that the development of multilayer clouds is favorable under warm and moist summer atmospheric conditions.

[28] There is little change in the average thickness of all clouds from summer to autumn. Cloud base and cloud top heights are higher in summer than in autumn. Cloud base and cloud top heights of the lowest layers in the two- and three-layer cloud configurations are closer to the surface in the summertime. However, the single-layer clouds and higher layers of the two- and three-layer clouds are located higher in the atmosphere during the summer.

4. Comparisons of Cloud Detection Using Different Instruments

[29] Differences in cloud boundaries derived from radiosonde and ground remote sensors are identified and compared.

4.1. Comparisons Between Radiosonde and WACR Cloud Boundaries

[30] The 95 GHz WACR was deployed at AMF-China from 15 October to 15 December 2008. Cloud statistics were not compiled from this cloud radar data set because not enough samples were obtained. However, the instrument's superior and more direct observational capability allows us to evaluate the radiosonde-based product. Even though a small number of observations were obtained, measurements from the WACR provided the first ever direct observation of clouds in China.

[31] ARM-developed cloud value-added products from the WACR are currently unavailable so contour plots of the distribution of clouds determined from RH measured by radiosondes and reflectivity measured by the WACR are shown in Figure 6. A macroscopic inspection of clouds detected from radiosonde profiles and by WACR shows that, although the two methods detect similar clouds, discrepancies emerge at a more detailed level. To latitudes above 12 km, there are several thin clouds in the radiosonde observations, which are not detected by the WACR. There are three possible reasons for this difference. First, objects detected by the radiosonde and WACR may be different because of radiosonde drift. Second, the method used to determine clouds from radiosonde observations may misclassify some clear moist layers as clouds or miss clouds altogether. Third, the WACR may fail to detect thin cloud layers [*Comstock et al.*, 2002; *Clothiaux et al.*, 2000].

[32] Figure 7 shows one case where four layers of cloud were detected by both instruments. A radiosonde was launched on 18 October at 1727 LST and reached an altitude of 14 km

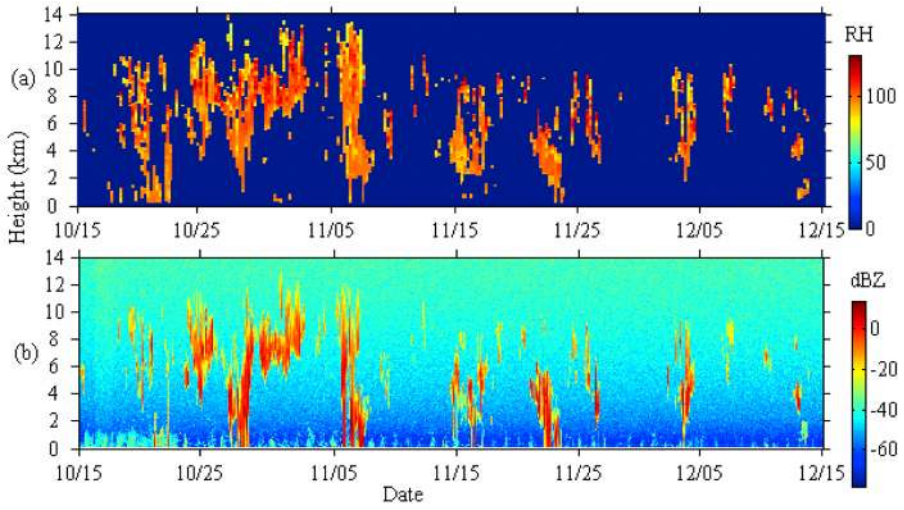

Figure 6. Cloud distributions measured by the (a) radiosonde and (b) reflectivity measured by the WACR.

at 1815 LST; the resulting RH profile is shown in Figure 7 (left). The radar reflectivities measured by the WACR are shown in Figure 7 (right). The solid red and black lines delineate radiosonde-measured cloud base and cloud top heights, respectively. The radiosonde classification of four layers of cloud is in good agreement with the WACR results.

4.2. Comparisons Between Radiosonde and MPL-Retrieved Cloud Boundaries

[33] The locations of cloud bases from radiosonde observations and from the MPL preliminary cloud base product were compared. Two factors were taken into account before comparing both data sets. First, the MPL may fail to detect upper cloud layers because of light extinction by lower layers of cloud so comparisons of data from the two instruments should not be limited to a particular time, but should be made during a time range. Second, the length of time a radiosonde spends taking measurements during its ascent in the atmosphere is about one and a half hours. So taking into account the two factors stated above and the difference caused by a drifting balloon and the fixed MPL, cloud base heights lower than 15 km, as determined by the radiosonde, are used for

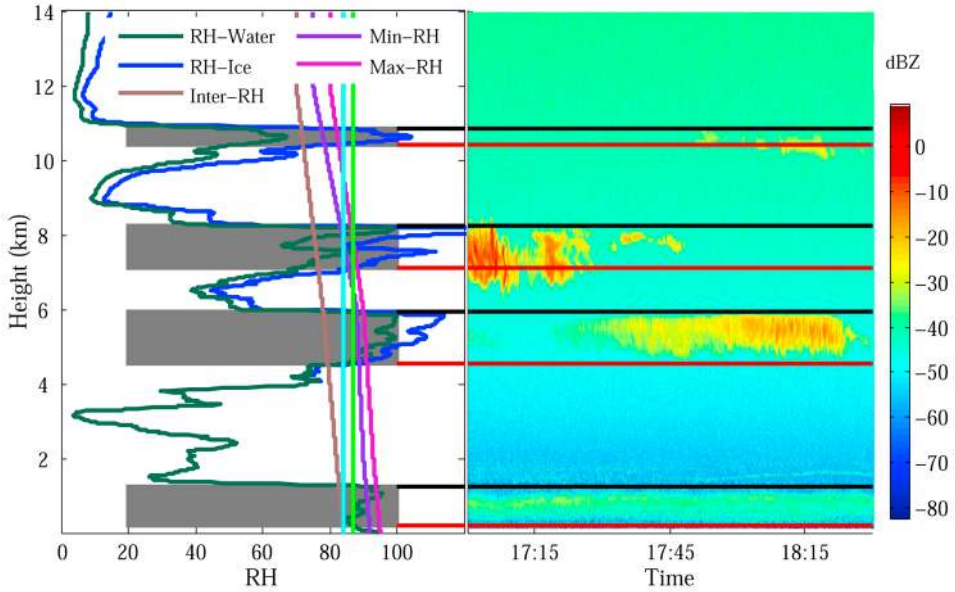

Figure 7. Detection of four layers of cloud by (left) the radiosonde and (right) the WACR. The solid red and black lines delineate radiosonde-measured cloud base and cloud top heights, respectively. In Figure 7 (left), the dark green line represents RH with respect to water, the blue line represents RH with respect to ice for levels with temperatures less than 0°C, and cyan and green lines represent the constant minimum and maximum RH thresholds of 84% and 87% reported in WR95. Sienna, purple, and pink lines represent inter-RH, min-RH, and max-RH thresholds as a function of altitude.

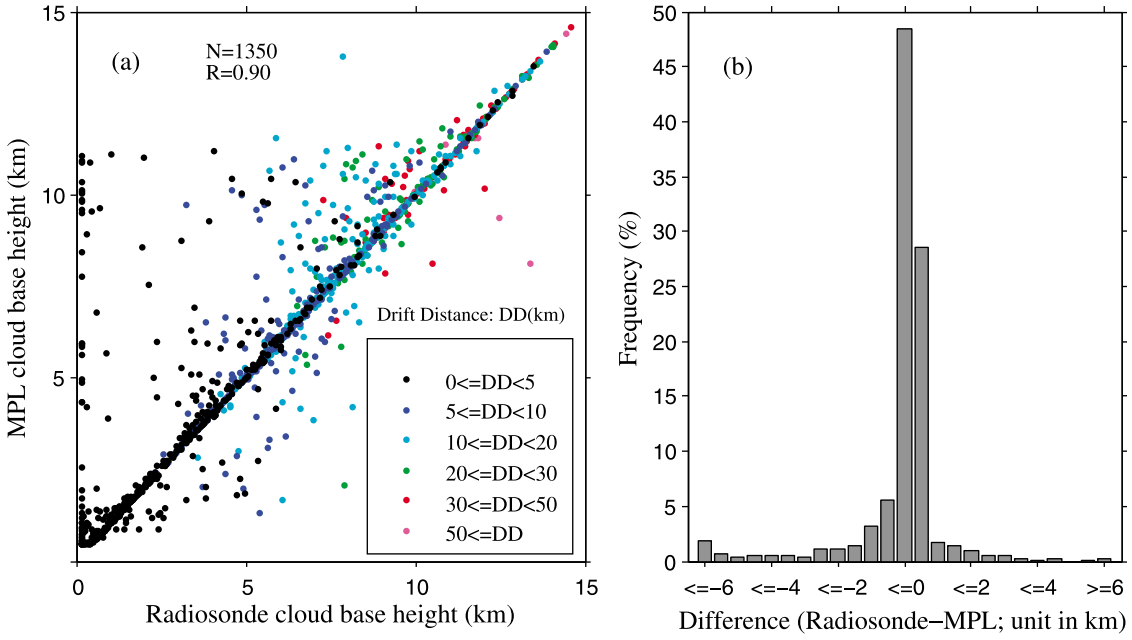

Figure 8. (a) Comparison of radiosonde and MPL cloud base heights. (b) Frequency distribution of cloud base height differences (Radiosonde-MPL).

comparison with the MPL preliminary cloud base product taken between 1 h before the balloon launch and 2 h after the launch. It is difficult to judge whether both instruments are detecting the same cloud layer or not. To ensure that both instruments are detecting the same cloud layer during a particular time period, MPL-derived cloud base results with the smallest absolute differences from radiosonde cloud base results are selected.

[34] On the basis of this, 1350 matched cloud layers are compared, accounting for 99.1% of all samples. The scatterplot of MPL cloud base heights as a function of radiosonde cloud base heights is shown in Figure 8a. Colored dots represent different radiosonde drift distances (DD). The frequency distribution of differences between radiosonde-derived and MPL-derived cloud base heights is shown in Figure 8b.

[35] Overall, cloud base heights detected by the two instruments agree very well, as indicated by the cluster of points along the 1:1 line; the correlation coefficient is 0.90. The outlier data near the 280 m point of the x axis corresponds to near-surface moist layers misclassified as cloud by the radiosonde. The absolute differences in cloud base heights from radiosonde and MPL data are less than 500 m for 77.1% of the cases analyzed. Of these cases, the average absolute difference is 90 m; the radiosonde tends to detect lower cloud bases. If the data cluster near the 280 m line is removed, the average absolute difference and bias between radiosonde and MPL cloud base heights are 503 and −226 m, respectively, and the correlation coefficient is now 0.93. The agreement between radiosonde-measured and MPL-retrieved cloud base heights is much better when the data cluster near the 280 m line is removed.

[36] There are still some cases where the cloud base heights derived from radiosonde and MPL measurements have large differences. Aside from errors in the radiosonde cloud detection method, there are three major factors that may explain these discrepancies. One factor involves balloon drift. Most balloon drift distances are more than 20 km with a maximum of about 200 km; drift distances between 20 and 200 km account for 70.6% of all cases. For greater than the 10 km point of the x axis in Figure 8a, there are several points with large differences. Radiosonde drift distances represented by these points are generally more than 30 km, which will affect the agreement between clouds results derived from the two instruments. Another factor involves the macro- and microphysical nature of lower level cloud layers. If the lower cloud layers are optically thick, upper layer clouds cannot be detected due to light extinction [*McGill et al.*, 2004]. The third factor is the dry bias at high altitudes that exists in RH measurements made by RS92 radiosondes [*Miloshevich et al.*, 2009]. Cloud layers at these altitudes might be missed by the radiosonde cloud determining method because of this dry bias.

4.3. Comparisons Between Radiosonde and Ceilometer Cloud Bases

[37] The ceilometer installed in the AMF can detect cloud bases lower than 8 km and can simultaneously detect up to three cloud layers. Radiosonde-measured cloud configurations with no more than three layers and with bases located below 7 km or the lowest three layers of multilayered clouds with bases located below 7 km were selected for comparison with ceilometer measurements. Five-hundred sixty-four matched cloud layer cases were identified from radiosonde/ceilometer observations. Figure 9 shows the scatterplot of ceilometer-measured cloud base height as a function of radiosonde-measured cloud base height and the frequency distribution of the differences between radiosonde-measured and ceilometer-measured cloud base heights. There is less agreement between cloud base heights measured by radiosonde and ceilometer than was seen in the comparisons between radiosonde and MPL measurements; the correlation

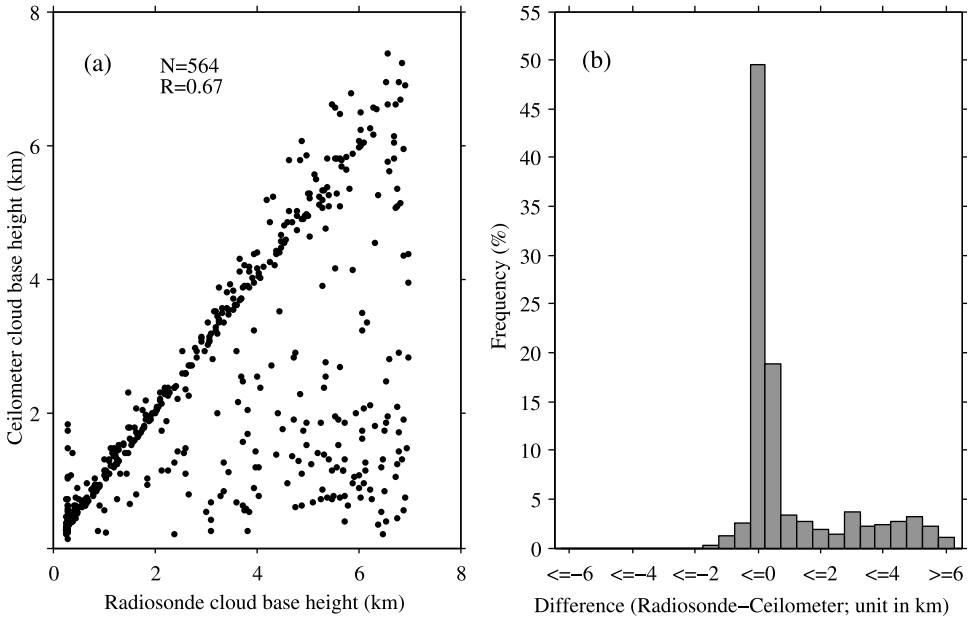

Figure 9. (a) Comparison of radiosonde and ceilometer cloud base heights. (b) Frequency distribution of cloud base height differences (Radiosonde-Ceilometer).

coefficient is 0.67. Radiosonde-detected cloud base heights appear systematically higher than those detected by the ceilometer. The average absolute difference between radiosonde and ceilometer measurements of cloud base heights is 990 m. The bias of 810 m indicates that the cloud base heights determined by radiosondes are higher than those measured by the ceilometer. Comparing Figure 9a with Figure 8a, there appears to be better agreement between radiosonde and ceilometer near-surface cloud detection. About 68.4% of the cases have absolute differences in cloud base heights within 500 m, which is less than the percentage of similar cases seen in comparisons between radiosonde and MPL data. Of these cases, the average absolute difference in cloud base heights is 97 m, and the bias is −58 m.

[38] Most of the scatter in Figure 9a corresponds to cases where radiosonde-measured cloud bases are higher than those measured by the ceilometer. The following two factors may explain the large discrepancies: (1) the presence of thick lower level clouds and fog, which affects the detection of upper level clouds by the ceilometer [*Clothiaux et al.*, 2000], and (2) balloon drift. The frequency distribution of differences between radiosonde and ceilometer cloud base locations is shown in Figure 10. Figure 10a represents single-layer clouds and the lowest layers from two- and

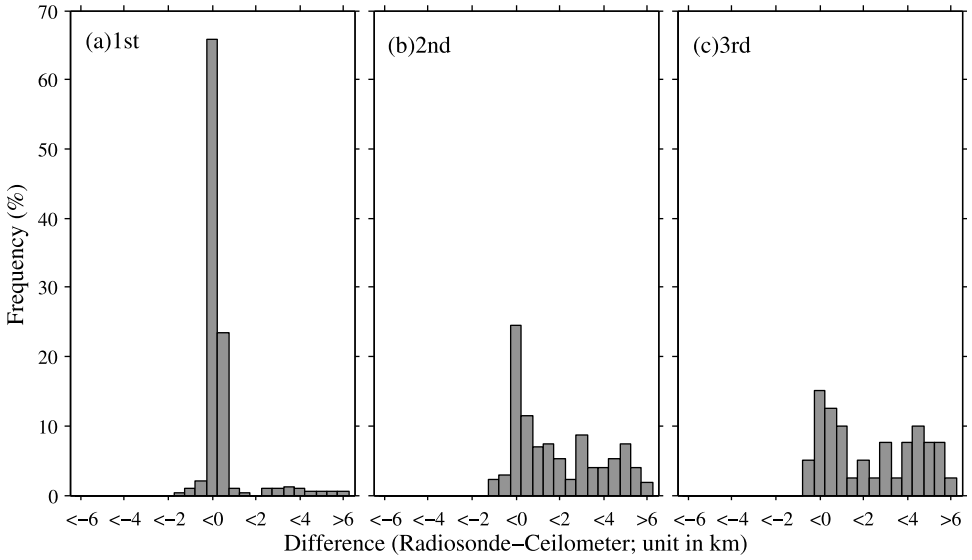

Figure 10. Frequency distribution of differences between radiosonde and ceilometer results for (a) first-layer, (b) second-layer, and (c) third-layer cloud.

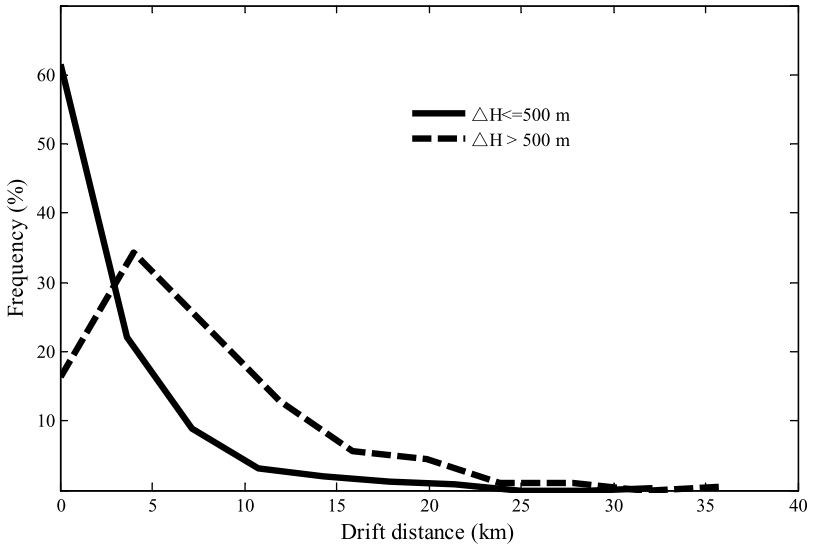

Figure 11. Balloon drift distributions for cases when the difference in cloud base height is less than or equal to 500 m and for cases when the difference in cloud base height is greater than 500 m.

three-layer cloud configurations and Figure 10b represents the highest layer from a two-layer cloud configuration and the middle layer of cloud in a three-layer cloud configuration. Figure 10c represents the highest layer of cloud in a three-layer cloud configuration. The frequency of differences within ±500 m for the first, second, and third layers of cloud is 89.4%, 36.0%, and 27.5%, respectively. Balloon drift distributions are shown in Figure 11, where the solid line represents balloon drift for cases where the absolute difference between the radiosonde and ceilometer cloud base heights is at most 500 m ($\Delta H \leq 500$ m) and the dashed line represents balloon drift for cases where the absolute difference is larger than 500 m ($\Delta H > 500$ m). It is clearly seen that the absolute difference between the radiosonde and ceilometer cloud base heights increases as the balloon drifts further (solid line to dashed line).

4.4. Comparisons Between MPL-Retrieved and the Ceilometer-Measured Cloud Bases

[39] Data are collected from both instruments at a high temporal resolution so only a portion of the data was selected in this analysis. Ceilometer-derived and MPL-derived cloud base results obtained during a 1 h period from the time of each radiosonde launch are selected. About 82.2% of the cases have absolute differences in cloud base heights within 500 m. Reasonable agreement is existed for much of the data, although there appears to be a systematic bias. A noticeable feature is that the MPL tends to retrieve higher cloud base heights than does the ceilometer. The ceilometer may fail to detect cloud layers higher in the atmosphere because the instrument uses a low energy beam that fades out much quicker than the MPL. Also moist layers near the surface are more often classified as clouds by the ceilometer than by the radiosonde or MPL. Algorithm differences can also yield biases in reported cloud base heights. One algorithm may identify a particular atmospheric structure as being a cloud layer, while another algorithm may not. The MPL uses a threshold variation method to identify the cloud bottom, and the ceilometer uses a calculated vertical visibility threshold of 100 m. This means that the ceilometer will not classify thin cloud regions that the MPL would identify.

[40] Different measurements of the cloud base heights of the cloud layers shown in Figure 7 are summarized in Table 4. The bias in cloud base height is largest between radiosonde and ceilometer measurements in this particular cloud case. Cloud boundaries determined by the radiosonde are more accurate if cloud layers are thicker.

5. Conclusions

[41] Knowledge of cloud vertical distribution is key for meteorological and climate studies. Direct observation of cloud vertical structure on a global scale has been inferred from CloudSat but the amount of information gleaned from this spaceborne platform is scanty because of its nadir view. Taking advantage of extensive measurements acquired during the AMF deployment at Shouxian, Anhui province from May to December of 2008, statistics regarding cloud vertical distribution at this site are presented. This is the first time in China that cloud boundaries derived from high temporal and vertical resolution radiosonde data have been compared to those derived from a suite of ground-based active sensors including cloud radar, micropulse lidar, and cloud ceilometer. Such rich information regarding cloud vertical distribution is unprecedented in the region.

Table 4. Cloud Base Heights Measured by Radiosonde, Ceilometer, and MPL Instruments[a]

Cloud Layer Base	Radiosonde	MPL	Ceilometer	R-M	R-C	M-C
Lowest layer base	186	555	1036	−369	−850	−481
Second layer base	4552	4707	5304	−155	−752	−597
Third layer base	7111	7180		−69		
Highest layer base	10414	10388		26		

[a]R-M, R-C, and M-C are the differences between the radiosonde and MPL measurements, radiosonde and ceilometer measurements, and MPL and ceilometer measurements, respectively. Units are in meters. R-M average = −141; R-C average = −801; M-C average = −539.

[42] The cloud detection method used in this study is based on the works of PWR95 and WR95 with some modification for application to data collected at Shouxian. The detection algorithm begins with the transformation of RH with respect to ice instead of liquid water for all levels with temperatures below 0°C. The RH profile is then examined to identify cloud layers following a series of tests based on both previous studies as well as modifications made in this study by virtue of active remote sensing data acquired at the site.

[43] Applying the detection method to 842 individual radiosonde atmospheric profiles, we derived the first comprehensive cloud vertical structure data set in China. The main findings are summarized as follows:

[44] 1. There were 1363 individual cloud layers identified from 14 May to 28 December 2008. One-, two-, and three-layer cloud configurations account for 28.0%, 25.8%, and 13.9% of the total samples, respectively. The percentage of low, middle, high, and deep convective clouds are 20.1%, 19.3%, 59.5%, and 1.1%, respectively, with high cloud layers being most prevalent.

[45] 2. Concerning all clouds, low clouds, middle clouds, and high clouds, their average cloud base heights are 5912, 714, 3558, and 8528 m, respectively. The mean cloud top heights are 7639, 2146, 5770, and 10042 m, respectively. The mean cloud thicknesses are 1727, 1432, 2212, and 1514 m, respectively.

[46] 3. The thicknesses of lower layers of clouds in a multilayer cloud are all smaller than the thicknesses of single-layer clouds with a mean difference of −867 m.

[47] 4. Maximum values of cloud top height and cloud thickness occurred at 1930 LST for single-layer clouds and for the uppermost layer of cloud in multiple-layer cloud configurations and at 1330 LST for the lowest layer of cloud in multiple-layer cloud configurations. The diurnal variations of the thickness of upper level clouds are larger than those of lower levels of clouds when multilayer clouds are present.

[48] 5. In general, the thickness of cloud layers does not change from summer to autumn. However, multilayer clouds are more frequent in the summer and cloud base and top heights are larger during the summertime than during the fall season.

[49] 6. Cloud detection based on radiosonde measurements compares very favorably with WACR image data except for a few cases where the WACR failed to detect thin clouds. The absolute differences in cloud base heights from radiosonde and MPL/ceilometer comparisons are less than 500 m for 77.1%/68.4% of the cases analyzed. The ceilometer fails to detect upper cloud layers due to the fast light extinction at lower altitudes.

[50] **Acknowledgments.** We would like to thank Yue-jian Xuan, Michael Alsop, Amon Haruta, and other participants for their contribution to the AMF program and Dr. Hong Guan for helpful discussions. We are also grateful to the work performed by the Meteorological Observation Center of the China Meteorological Administration and the Anhui Meteorological Bureau toward the AMF program. We also thank those responsible for obtaining the radiosonde data: Changqun Ma, Yizhen Quan, and Xin Qi. We highly value the publicly available data that were made available by the Atmospheric Radiation Measurement (ARM) Program sponsored by the U.S. Department of Energy. This work is supported by National Natural Science Foundation of China under grant 40830102, MOST (2006CB403706 and 2010CB950804), DOE (DEFG0208ER64571-S01), NASA (NNX08AH71G-), and DOE/ARM.

References

Alduchov, O. A., and E. E. Eskridge (1996), Improved Magnus' form approximation of saturation vapor pressure, *J. Appl. Meteorol.*, *35*, 601–609.

Arabey, E. N. (1975), Radiosounding data as means for cloud layers revealing cloud layer (in Russian), *Meteorol. Gidrol.*, *6*, 23–37.

AWS (1979), *The Use of the Skew of T, Log P Diagram in Analysis and Forecasting*, 150 pp., *Air Weather Service Tech. Rep., AWS/TR-79/006*, Scott AFB, Ill.

Blaskovic, M., R. Davies, and J. B. Snider (1991), Diurnal variation of marine stratocumulus over San Nicolas Island during July 1987, *Mon. Weather Rev.*, *119*, 1469–1478.

Chang, F.-L., and Z. Li (2005a), A new method for detection of cirrus overlapping water clouds and determination of their optical properties, *J. Atmos. Sci.*, *62*, 3993–4009.

Chang, F.-L., and Z. Li (2005b), A comparison of the global surveys of high, mid, and low clouds from satellites and general circulation models, in *Proceedings of the Fifteenth Atmospheric Radiation Measurement (ARM) Science Team Meeting, Daytona Beach, Florida, 14–18 March 2005*, U.S. Dep. of Energy, Washington, D. C.

Chen, C., and W. R. Cotton (1987), The physics of the marine stratocumulus-capped mixed layer, *J. Atmos. Sci.*, *44*, 2951–2977.

Chernykh, I. V. (1999), Averages of relative humidity at the cloud base level, *WMO Rep. 28, WMO/TD 942*, pp. 2.7–2.8.

Chernykh, I. V., and R. E. Eskridge (1996), Determination of cloud amount and level from radiosonde soundings, *J. Appl. Meteorol.*, *35*, 1362–1369.

Chernykh, I. V., O. A. Alduchov, and R. E. Eskridge (2000), Trends in low and high cloud boundaries and errors in height determination of cloud boundaries, *Bull. Am. Meteorol. Soc.*, *82*(9), 1941–1947.

Clothiaux, E. E., T. P. Ackerman, G. C. Mace, K. P. Moran, R. T. Marchand, M. A. Miller, and B. E. Martner (2000), Objective determination of cloud heights and radar reflectivities using a combination of active remote sensors at the ARM CART sites, *J. Appl. Meteorol.*, *39*, 645–665.

Comstock, J. M., T. P. Ackerman, and G. G. Mace (2002), Ground-based lidar and radar remote sensing of tropical cirrus clouds at Nauru Island: Cloud statistics and radiative impacts, *J. Geophys. Res.*, *107*(D23), 4714, doi:10.1029/2002JD002203.

Dolgin, M. I. (1983), Determine scheme clouds from atmosphere sounding in Antarctic Continent (in Russian), *Meteorol. Gidrol.*, *11*, 47–51.

Dong, X., P. Minnis, T. P. Ackerman, E. E. Clothiaux, G. C. Mace, C. N. Long, and J. C. Liljegren (2000), A 25-month database of stratus cloud properties generated from ground-based measurements at the Atmospheric Radiation Measurement Southern Great Plains Site, *J. Geophys. Res.*, *105*(D4), 4529–4537, doi:10.1029/1999JD901159.

Dong, X., P. Minnis, and B. Xi (2005), A climatology of midlatitude continental clouds from ARM SGP site: Part I. Low-level cloud macrophysical, microphysical and radiative properties, *J. Clim.*, *18*, 1391–1410.

Dong, X., B. Xi, and P. Minnis (2006), A climatology of midlatitude continental clouds from ARM SGP site: Part II. Cloud fraction and surface radiative forcing, *J. Clim.*, *19*, 1765–1783.

Guan, H., M. K. Yau, and R. Davies (1997), The effects of longwave radiation in a small cumulus cloud, *J. Atmos. Sci.*, *54*, 2201–2214.

Han, D., and R. G. Ellingson (2000), An experimental technique for testing the validity of cumulus cloud parameterisations for longwave radiation calculations, *J. Appl. Meteorol.*, *39*, 1147–1159.

Lazarus, S. M., S. K. Krueger, and G. G. Mace (2000), A cloud climatology of the Southern Great Plains ARM CART, *J. Clim.*, *13*, 1762–1775.

Mace, G. G., Q. Zhang, M. Vaughan, R. Marchand, G. Stephens, C. Trepte, and D. Winker (2009), A description of hydrometeor layer occurrence statistics derived from the first year of merged Cloudsat and CALIPSO data, *J. Geophys. Res.*, *114*, D00A26, doi:10.1029/2007JD009755.

Marchand, R. T., T. P. Ackerman, M. D. King, C. Moroney, R. Davies, J.-P. A. L. Muller, and H. Gerber (2001), Multiangle observations of arctic clouds from FIRE ACE: June 3, 1998, case study, *J. Geophys. Res.*, *106*(D14), 15,201–15,214, doi:10.1029/2000JD900302.

McGill, M. J., et al. (2004), Combined lidar-radar remote sensing: Initial results from CRYSTAL-FACE, *J. Geophys. Res.*, *109*, D07203, doi:10.1029/2003JD004030.

Miloshevich, L. M., H. Vömel, D. N. Whiteman, and T. Leblanc (2009), Accuracy assessment and correction of Vaisala RS92 radiosonde water vapor measurements, *J. Geophys. Res.*, *114*, D11305, doi:10.1029/2008JD011565.

Minnis, P., and E. F. Harrison (1984), Diurnal variability of regional cloud and clear-sky radiative parameters derived from GOES data: Part I. Analysis method, *J. Clim. Appl. Meteorol.*, *23*, 993–1011.

Minnis, P., Y. Yi, J. Huang, and J. K. Ayers (2005), Relationships between radiosonde and RUC-2 meteorological conditions and cloud occurrence determined from ARM data, *J. Geophys. Res.*, *110*, D23204, doi:10.1029/2005JD006005.

Naud, C., J.-P. Muller, and E. E. Clothiaux (2003), Comparison between active sensor and radiosonde cloud boundaries over the ARM Southern Great Plains site, *J. Geophys. Res.*, *108*(D4), 4140, doi:10.1029/2002JD002887.

Okamoto, H., T. Nishizawa, T. Takemura, K. Sato, H. Kumagai, Y. Ohno, N. Sugimoto, A. Shimizu, I. Matsui, and T. Nakajima (2008), Vertical cloud properties in the tropical western Pacific Ocean: Validation of the CCSR/NIES/FRCGC GCM by shipborne radar and lidar, *J. Geophys. Res.*, *113*, D24213, doi:10.1029/2008JD009812.

Ou, S. C., K. N. Liou, and T. R. Caudill (1998), Remote sounding of multilayer cirrus cloud systems using AVHRR data collected during FIRE-II-IFO, *J. Appl. Meteorol.*, *37*, 241–254.

Poore, K. D., J. Wang, and W. Rossow (1995), Cloud layer thickness from a combination of surface and upper air observations, *J. Clim.*, *8*, 550–568.

Rogers, D. P., and D. Koracin (1992), Radiative transfer and turbulence in the cloud topped marine atmospheric boundary layer, *J. Atmos. Sci.*, *49*, 1473–1486.

Slingo, J. M. (1980), A cloud parametrization scheme derived from GATE data for use with a numerical model, *Q. J. R. Meteorol. Soc.*, *106*, 747–770.

Stephens, G. L., et al. (2002), The CloudSat mission and the A-TRAIN: A new dimension to space-based observations of clouds and precipitation, *Bull. Am. Meteorol. Soc.*, *83*, 1771–1790.

Wang, J. (1997), Determination of cloud vertical structure from upper air observations and its effects on atmospheric circulation in a GCM, Ph.D. Thesis, 233 pp., Columbia Univ., New York.

Wang, J., and W. B. Rossow (1995), Determination of cloud vertical structure from upper air observations, *J. Appl. Meteorol.*, *34*, 2243–2258.

Wang, J., W. B. Rossow, T. Uttal, and M. Rozendaal (1999), Variability of cloud vertical structure during ASTEX observed from a combination of rawinsonde, radar, ceilometer, and satellite, *Mon. Weather Rev.*, *127*, 2482–2502.

Wang, J., W. B. Rossow, and Y. Zhang (2000), Cloud vertical structure and its variations from a 20 year global rawinsonde data set, *J. Clim.*, *13*, 3041–3056.

Webster, P. J., and G. L. Stephens (1984), Cloud-radiation interaction and the climate problem, in *The Global Climate*, edited by J. T. Houghton, pp. 63–78, Cambridge Univ. Press, New York.

Xi, B., X. Dong, P. Minnis, and M. M. Khaiyer (2010), A 10 year climatology of cloud fraction and vertical distribution derived from both surface and GOES observations over the DOE ARM SPG site, *J. Geophys. Res.*, *115*, D12124, doi:10.1029/2009JD012800.

H. Chen, X. Fan, L. Peng, Y. Yu, and J. Zhang, Key Laboratory of Middle Atmosphere and Global Environment Observation, Institute of Atmospheric Physics, Chinese Academy of Sciences, Beijing 100029, China.

M. Cribb and Z. Li, Earth System Science Interdisciplinary Center, Department of Atmospheric and Oceanic Science, University of Maryland, 5825 University Research Ct., Ste. 4001, College Park, MD 20742, USA. (zli@atmos.umd.edu)